

# Electric-field control of collective spin excitations in Néel-type skyrmions

Hong-Bo Chen<sup>1</sup> and You-Quan Li<sup>2,3</sup>

<sup>1</sup>*Ningbo Institute of Technology, Zhejiang University, Ningbo 315100, China*

<sup>2</sup>*Zhejiang Institute of Modern Physics and Department of Physics, Zhejiang University, Hangzhou 310027, China*

<sup>3</sup>*Collaborative Innovation Center of Advanced Microstructures, Nanjing University, Nanjing 210093, China*

We demonstrate that an electric field could activate the three low-energy eigenmodes of the Néel-type skyrmion lattice via the electrically induced Dzyaloshinskii-Moriya interaction. In particular, we predict that the relative intensity of the clockwise rotation mode against the counter-clockwise rotation mode is significantly enhanced for the electrical activation in comparison with the magnetic activation. We also discover that the electrically and magnetically active modes obey unique selection rules. These findings promise a fresh pathway towards energy-efficient electrical manipulation of skyrmion excitations for future skyrmion-based magnonics.

Magnetic skyrmions are nanoscale, topologically stable spin textures.<sup>1</sup> Because of their unique feature of topology and controllable manipulation, they are in the focus of current research and an emerging area for building highly efficient next-generation spintronic devices.<sup>2–5</sup> Three distinct classes of magnetic skyrmions have by now been experimentally discovered, namely, Bloch skyrmion,<sup>6–8</sup> Néel skyrmion,<sup>9,10</sup> and antiskyrmion,<sup>11</sup> which can be stabilized by the bulk, interfacial, and anisotropic Dzyaloshinskii-Moriya interaction (DMI),<sup>12</sup> respectively. Controlling of magnetic skyrmions is an essential issue regarding their potential application in devices. Nowadays, various schemes have been demonstrated such as, the use of electric currents,<sup>13–18</sup> temperature gradient,<sup>19–21</sup> microwaves,<sup>22,23</sup> or strain.<sup>24</sup> In particular, manipulating magnetic skyrmions by an electric field has been achieved through the voltage-controlled magnetic anisotropy in ultrathin metal films<sup>25,26</sup>, or the magnetoelectric coupling in multiferroic insulator.<sup>27,28</sup> Moreover, a very intriguing electric-field induced DMI mechanism has recently been demonstrated<sup>29,30</sup> to control the skyrmion dynamics.

Meanwhile, intense activity has been devoted to the collective spin excitations of skyrmions, which is promising for the potential application in the field of magnonics.<sup>31,32</sup> The fundamental eigenmodes of skyrmions can be excited usually by an ac magnetic field. In the skyrmion crystal phase, three distinctive low-energy eigenmodes, i.e., the breathing (BR) mode, the clockwise (CW), and the counter-clockwise (CCW) rotation modes, have been first revealed theoretically by Mochizuki<sup>33</sup> and subsequently demonstrated experimentally in both Bloch<sup>34–36</sup> and Néel<sup>37,38</sup> skyrmions. The two rotational modes CW and CCW are characterized by the core of skyrmion rotates simultaneously clockwise and counter-clockwise, respectively, under an in-plane ac magnetic field, while the breathing mode is excited by an out-of-plane ac field with the skyrmion expanding and shrinking coherently. Currently, skyrmion excitations have been examined primarily by means of microwave magnetic fields. Therefore, seeking mechanisms that enable electric-field controlled skyrmion excitations are particularly attractive since electric field is much eas-

ier to manipulate than magnetic field. A natural way is to use the magnetoelectric coupling in insulator, which has recently achieved in a multiferroic Bloch-type skyrmion  $\text{Cu}_2\text{OSeO}_3$ .<sup>39,40</sup> However, for widely existing Néel-type skyrmions, this has rarely been explored before and remains an outstanding theoretical issue.

In this work we aim at exploring the effect that an electric field can have on the collective spin excitations in the Néel-type skyrmions. To study this, we employ a novel electric-field induced DMI mechanism developed recently.<sup>41–43</sup> This coupling can also be considered as the spin flexoelectric effect.<sup>44</sup> We demonstrate the electrical activation of spin excitations in the Néel skyrmion lattice and determine the spectrum of three eigenmodes. We predict that the higher-lying CW rotation mode, absent in the previous conventional microwave magnetic field experiments, would be easily observed in the microwave electric field experiment because its relatively strong spectral weight driven by the ac electric field. Additionally, we discover that the same skyrmion-mode excited simultaneously by the electric and magnetic field obeys the identical selection rule, which is totally different from that of the Bloch-type skyrmions.

We consider a classical spin model on a two-dimensional square lattice in the  $x$ - $y$  plane. The effective Hamiltonian supporting the Néel skyrmion is given by

$$H_0 = - \sum_{\langle i,j \rangle} [J \mathbf{S}_i \cdot \mathbf{S}_j + \mathbf{D}_{ij} \cdot (\mathbf{S}_i \times \mathbf{S}_j)] - \sum_i \mathbf{B} \cdot \mathbf{S}_i, \quad (1)$$

where  $\mathbf{S}_i$  is the normalised spin at the site  $i$ , and the summation  $\langle i, j \rangle$  runs over all pairs of nearest-neighbour spins.  $J > 0$  is the ferromagnetic exchange coupling,  $\mathbf{B}$  is the external magnetic field for  $\mathbf{B} = B\hat{z}$ , and  $\mathbf{D}_{ij} = D\hat{z} \times \hat{\mathbf{r}}_{ij}$  is the intrinsic interfacial DMI with  $\hat{\mathbf{r}}_{ij}$  the unit vector from spins  $i$  to  $j$ , the DM constant  $D = J \tan(2\pi/p)$  defining the pitch length ( $p$ ) of the modulated spin structures. In what follows, we fix the exchange constant  $J = 1$  for the energy units, and the DM value with  $D/J = 0.445$  corresponding to the pitch length  $p = 15$ . The calculations were performed on a  $66 \times 66$  lattices with periodic boundary conditions imposed along  $x$ - and  $y$ - direction.

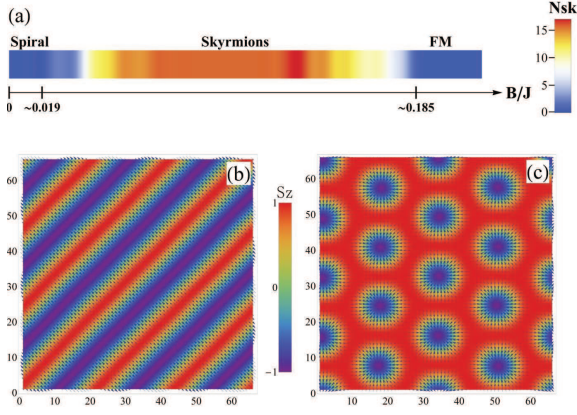


FIG. 1. (color online) (a) Ground-state phase diagram of the model (1) as a function of the external magnetic field  $\mathbf{B} = B\hat{z}$ . Three distinct spin phases, spiral state, skyrmions state and ferromagnetic (FM) state are appeared. The color depicts the calculated cumulative skyrmion number  $N_{\text{sk}}$ . (b),(c) Representative ground-state spin textures of the system: (b) spiral state for  $B/J = 0.0$ , (c) skyrmion lattice state for  $B/J = 0.11$ . The arrows represent the in-plane components of spins and the color indicates their  $z$  components.

We computed the time evolution of the spin dynamics by solving the Landau-Lifshitz-Gilbert (LLG) equation, which is written as<sup>33</sup>

$$\frac{\partial \mathbf{S}_i}{\partial t} = -\frac{1}{1 + \alpha^2} \left[ \mathbf{S}_i \times \mathbf{H}_i^{\text{eff}} + \frac{\alpha}{S} \mathbf{S}_i \times (\mathbf{S}_i \times \mathbf{H}_i^{\text{eff}}) \right], \quad (2)$$

where  $\alpha$  is the Gilbert-damping parameter, and  $\mathbf{H}_i^{\text{eff}} = -\partial H / \partial \mathbf{S}_i$  is the effective local field acting on the  $i$ th spin  $\mathbf{S}_i$ .  $H = H_0 + H_E(t)$ ,  $H_0$  is the spin model Hamiltonian given by Eq. (1), while the term  $H_E(t) = \gamma(\mathbf{E}(t) \times \hat{\mathbf{r}}_{ij}) \cdot (\mathbf{S}_i \times \mathbf{S}_j)$  represents the electric-field induced DMI,<sup>41–43,45</sup> with the coupling constant  $\gamma = Jea/E_{\text{SO}}$ , where  $e$  is the electron charge,  $a$  is the lattice constant, and  $E_{\text{SO}}$  is an energy scale associated with the inverse of the strength of the spin-orbit coupling. Given the typical parameter values,  $J \sim 1\text{meV}$ ,  $a \sim 10\text{\AA}$ , and  $E_{\text{SO}} \sim 1\text{eV}$ , we roughly estimate  $\gamma \sim 10^{-31}$  Cm. Each classical spin  $\mathbf{S}_i$  is taken to have the unit length,  $S = 1$ . For the value of  $\alpha$ , we adopt  $\alpha = 0.04$  and  $0.005$  for simulations of the phase diagram and the dynamic response of system to the applied ac fields, respectively. We use the fourth-order Runge-Kutta method for numerical integration of the LLG equation (2).

Figure 1 shows the phase diagram at zero temperature of the spin model (1) as a function of magnetic field  $B$ , and two representative spin textures of the phases. The phase diagram is obtained from the combination of the classical Monte-Carlo simulations and the LLG equation. We first start with the Monte-Carlo simulated annealing for the model (1) to obtain stable spin states until a low temperature ( $k_B T/J = 0.01$ ) is reached. Then, using the LLG equation, we further relax them by sufficient time evolution to obtain its ground-state. The skyrmions state

in the system can be recognised effectively by a nonzero skyrmion number (topological charge), which is given by

$$N_{\text{sk}} = \frac{1}{4\pi} \int dx dy \mathbf{S} \cdot (\partial_x \mathbf{S} \times \partial_y \mathbf{S}). \quad (3)$$

In practice for a square lattice, we compute the discretized version of this expression.<sup>46,47</sup> Figure 1(a) reveals that three different types of spin states, specifically, spiral state, skyrmions state, and the ferromagnetic (FM) state successively emerge as  $B$  increasing. The colors in the phase diagram indicate the calculated total skyrmion number, which is a measure for the total number of skyrmions in the system. We note that the spiral and FM phases have a zero skyrmion number. The phase boundary between the spiral phase and the skyrmions phase is at  $B/J \sim 0.019$ , and that between the skyrmions and the ferromagnetic phase is at  $B/J \sim 0.185$ . Figures 1(b) and (c) display the representative spin textures of spiral and skyrmion lattice phases for  $B/J = 0.0$  and  $0.11$ , respectively. The skyrmion lattice phase shown in Fig. 1 (c) will be used to simulate the spin excitations in the follows.

To study the spin excitations of the system, we calculate the dynamical susceptibilities, which are defined

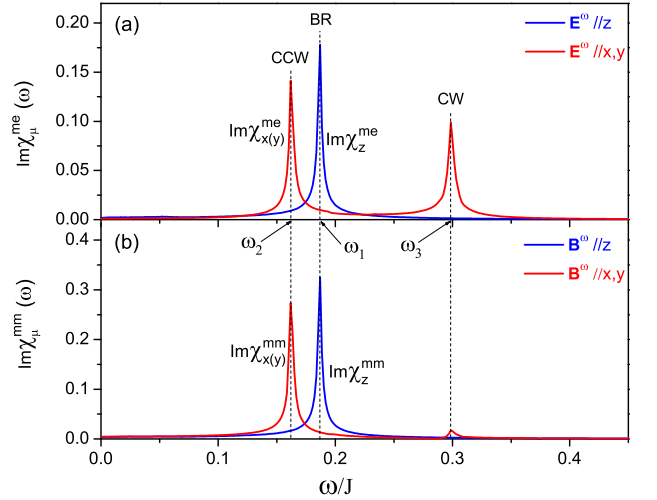


FIG. 2. (color online) (a) Imaginary parts of the dynamical electromagnetic susceptibilities  $\text{Im}\chi_{\mu}^{\text{me}}(\omega)$  ( $\mu = x, y, z$ ) obtained after applying a  $\delta$ -function electric field pulse  $\mathbf{E}(t) = \delta(t)\mathbf{E}^{\omega}$  to the stable skyrmion lattice state [Fig. 1(c)], where  $\text{Im}\chi_{x(y)}^{\text{me}}(\omega)$  and  $\text{Im}\chi_z^{\text{me}}(\omega)$  for  $\mathbf{E}^{\omega} \parallel \hat{x}(\hat{y})$  and  $\mathbf{E}^{\omega} \parallel \hat{z}$ , respectively. The three resonant modes were ascribed to the BR, CCW, and CW mode, which are located at  $\omega_1/J = 0.1869$ ,  $\omega_2/J = 0.1618$ , and  $\omega_3/J = 0.2985$ , respectively. (b) The imaginary parts of the dynamical magnetic susceptibilities,  $\text{Im}\chi_{x(y)}^{\text{mm}}(\omega)$  and  $\text{Im}\chi_z^{\text{mm}}(\omega)$  for  $\mathbf{B}^{\omega} \parallel \hat{x}(\hat{y})$  and  $\mathbf{B}^{\omega} \parallel \hat{z}$ , respectively. Comparison between the spectra of  $\text{Im}\chi_{\mu}^{\text{me}}(\omega)$  and  $\text{Im}\chi_{\mu}^{\text{mm}}(\omega)$ , the electrically and magnetically active resonances are located at the identical frequencies with the same selection rules.

as<sup>33</sup>

$$\chi_{\mu}^{\text{mm}}(\omega) = \frac{\Delta S_{\mu}(\omega)}{B_{\mu}(\omega)}, \quad \chi_{\mu}^{\text{me}}(\omega) = \frac{\Delta S_{\mu}(\omega)}{E_{\mu}(\omega)}, \quad (4)$$

where the subscript  $\mu$  stands for  $x$ ,  $y$  or  $z$ .  $B_{\mu}(\omega)$  and  $E_{\mu}(\omega)$  are the Fourier transform of the time-dependent pulse of magnetic field  $B_{\mu}(t)$  and electric field  $E_{\mu}(t)$  applied in the  $\mu$  direction, respectively. Here, we employ a time-localized, uniform  $\delta$ -function pulse, i.e.,  $\mathbf{E}(t) = \delta(t)\mathbf{E}^{\omega}$  applied at  $t = 0$ . And  $\Delta S_{\mu}(\omega)$  is the Fourier transform of the  $\mu$ -component of the spatially averaged spin  $\Delta \mathbf{S}(t) = \mathbf{S}(t) - \mathbf{S}(0)$ , with  $\mathbf{S}(t) = (1/N) \sum_{i=1} \mathbf{S}_i(t)$ , which is the transient response of the system under the intense pulse of external fields. In the LLG simulation, we use a smaller value of the damping constant,  $\alpha = 0.005$ , which is allowed for better frequency resolution of the excited modes.

Figure 2 shows the imaginary parts of the dynamical susceptibilities for the selected skyrmion lattice (Fig. 1 c) under an in-plane and out-of-plane  $\delta$ -function pulse of electric and magnetic field. In Fig. 2(a), we firstly display the imaginary parts of the dynamical electro-magnetic susceptibilities  $\text{Im} \chi_{\mu}^{\text{me}}(\omega)$ , with  $\text{Im} \chi_z^{\text{me}}(\omega)$  and  $\text{Im} \chi_{x(y)}^{\text{me}}(\omega)$  for the out-of-plane ac electric field  $\mathbf{E}^{\omega} \parallel \hat{z}$  and in-plane ac electric field  $\mathbf{E}^{\omega} \parallel \hat{x}(\hat{y})$ , respectively. We can see that three resonant peaks are clearly exhibited. In  $\text{Im} \chi_z^{\text{me}}(\omega)$  for  $\mathbf{E}^{\omega} \parallel \hat{z}$ , we observe a single resonant peak centered at  $\omega_1/J = 0.1869$ . As will be justified in detail below in Fig. 3 (a), this resonant mode can be identified as the so-called breathing mode, where all the skyrmions in the skyrmion lattice periodically shrink and expand in a uniform way under the out-of-plane driving electric field. We should note that this electrically activated breathing mode has also been identified very recently.<sup>45</sup> Furthermore, in  $\text{Im} \chi_{x(y)}^{\text{me}}(\omega)$  for  $\mathbf{E}^{\omega} \parallel \hat{x}(\hat{y})$ , we see two distinct resonant peaks, a lower-lying peak located at  $\omega_2/J = 0.1618$ , and a higher-lying peak at  $\omega_3/J = 0.2985$ . In fact, as will be shown in Figs. 3(b) and 3(c), the lower-lying mode ( $\omega_2$ ) can be assigned to the CCW rotation mode, while the higher-lying mode ( $\omega_3$ ) to the CW rotation mode, where all skyrmion cores rotate simultaneously counter-clockwise or clockwise under the in-plane driving electric field.

For comparison, we also present in Fig. 2(b) the imaginary parts of the calculated magnetic susceptibilities,  $\text{Im} \chi_{x(y)}^{\text{mm}}(\omega)$  and  $\text{Im} \chi_z^{\text{mm}}(\omega)$  for the in-plane magnetic field  $\mathbf{B}^{\omega} \parallel \hat{x}(\hat{y})$  and the out-of-plane  $\mathbf{B}^{\omega} \parallel \hat{z}$ , respectively. Three magnetically active resonance modes are also clearly observed, which are consistent with previous experimental observations<sup>37,38</sup> as well as theoretical investigations<sup>33,48</sup>. Compared to the spectra of  $\text{Im} \chi_{\mu}^{\text{me}}(\omega)$  in Fig. 2(a), one can find that three electrically active resonances can be seen in the spectra of corresponding magnetic susceptibilities  $\text{Im} \chi_{\mu}^{\text{mm}}(\omega)$  at the identical frequencies. This means that both the electric and magnetic fields excite the same modes with the same selection rules, which is in striking contrast

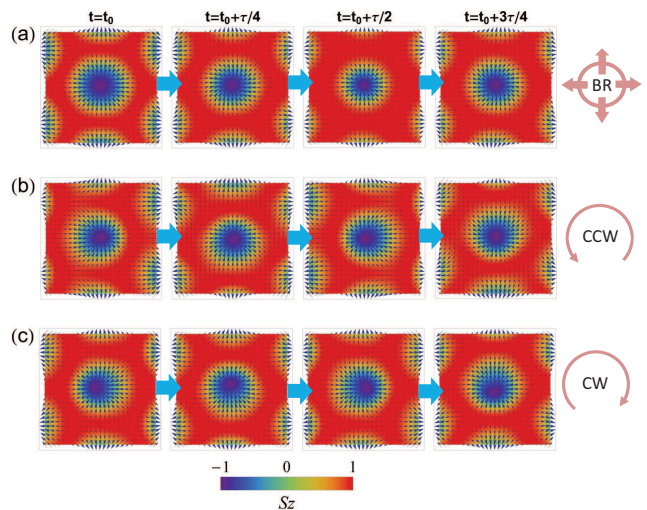


FIG. 3. (color online) Time evolution snapshots of the spatial spin profiles for a constituent skyrmion of the skyrmion lattice phase [Fig. 1(c)] induced by an oscillating sinusoidal electric field, with a time increment of  $1/4$  of the oscillation period  $\tau$ . The arrows denote the in-plane spin components, while the contour plot represents the out-of-plane  $z$  component. (a) The breathing mode excited by an out-of-plane oscillating electric field  $\mathbf{E}(t) = E_z^{\omega} \sin(\omega_1 t) \hat{z}$  with field amplitude  $\gamma E_z^{\omega} = 0.006$ . (b) The CCW rotation mode excited by an in-plane oscillating electric field  $\mathbf{E}(t) = E_x^{\omega} \sin(\omega_2 t) \hat{x}$  with  $\gamma E_x^{\omega} = 0.015$ . (c) The CW rotation mode excited by  $\mathbf{E}(t) = E_x^{\omega} \sin(\omega_3 t) \hat{x}$  with  $\gamma E_x^{\omega} = 0.015$ .

to the case of multiferroic  $\text{Cu}_2\text{OSeO}_3$  hosting Bloch-type skyrmions where the same skyrmion-mode active to both the electric and magnetic field obeys a different selection rule.<sup>39</sup> Moreover, we should note that the higher-lying CW mode was not easily detected experimentally via the microwaves magnetic field<sup>34,35,38</sup> due to its rather weak spectra intensity according to the theoretical calculations.<sup>33,38</sup> However, one can find in Fig. 2(a) that the relative intensity of the CW mode against the CCW mode in  $\text{Im} \chi_{x(y)}^{\text{me}}$  is significantly enhanced under the ac electric fields. Therefore, our simulations indicate that the CW mode is expected to be identified experimentally through the microwave electric field.

To exclusively classify each electrically active modes revealed in the spectra of Fig. 2(a), we examine the spin dynamics of the skyrmion lattice under a spatially uniform sinusoidal electric field  $\mathbf{E}(t) = \mathbf{E}^{\omega} \sin(\omega_i t)$ , where  $\omega_i$  ( $i = 1-3$ ) are the corresponding eigenfrequencies of the skyrmion excitations, by numerically solving the LLG equation. The Gilbert-damping constant is fixed at  $\alpha = 0.005$ . Since for each mode, all the skyrmions in the skyrmion lattice behaves uniformly the same way, we focus on a constituent skyrmion. The selected constituent skyrmion is between the sites  $22 \leq i_x \leq 47$ , and  $20 \leq i_y \leq 45$  shown in Fig. 1(c).

In Fig. 3, we depict four time representative snapshots of the simulated spin texture evolution of a constituent

skyrmion for three electrically active eigenmodes, over one oscillation period  $\tau$ . The characteristic motions of the three eigenmodes are clearly illustrated in the respective time evolutions of their dynamic spatial spin profiles. In Fig. 3(a), we show the simulated spin dynamics of a constituent skyrmion excited by an out-of-plane oscillating electric field  $\mathbf{E}(t) = E_z^\omega \sin(\omega_1 t) \hat{z}$  with field amplitude  $\gamma E_z^\omega = 0.006$ . The size of each constituent skyrmion in the lattice performs an oscillatingly shrinking and expanding motion, so it can be unambiguously assigned to the breathing mode of the skyrmion lattice. In Figs. 3(b) and (c), we applied an in-plane oscillating electric field  $\mathbf{E}(t) = E_x^\omega \sin(\omega_i t) \hat{x}$  with field amplitude  $\gamma E_x^\omega = 0.015$ , and the resonant frequencies  $\omega_i$  fixed for the lower-lying mode  $\omega_2$  and the higher-lying mode  $\omega_3$ , respectively. In Fig. 3(b), we can see that the spin profiles rotate in the sense of counter-clockwise for the lower-lying mode  $\omega_2$ , while in Fig. 3(c) for the higher-lying mode  $\omega_3$  the rotation sense is clockwise. Therefore, the mode  $\omega_2$  and mode  $\omega_3$  can be assigned to the CCW and CW rotation mode, respectively.

In conclusion, we have theoretically demonstrated the electric-field control of collective spin excitations of the Néel-type skyrmion lattice phase, driven by an electrically induced DMI effect. We successfully identified the three eigenmodes of the Néel-type skyrmion lattice by using the electric field. Furthermore, we revealed that the higher-lying CW rotation mode excited by the electric field has a relatively strong spectral intensity. We also showed that the same skyrmion-mode activated simultaneously by the electric and magnetic field exhibits the same selection rule. These features are expected to bring in a new insight to electrically activate spin excitations of magnetic skyrmions.

## ACKNOWLEDGMENTS

We acknowledge support by the National Key R & D Program of China (No. 2017YFA0304304), NSFC (Nos. 11547102 and 11604294), Zhejiang Provincial Natural Science Foundation of China (No. LY16A040008), and Ningbo Natural Science Foundation (2015A610003).

- <sup>1</sup>U. K. Röbner, A. N. Bogdanov, and C. Pfleiderer, *Nature* **442**, 797 (2006).
- <sup>2</sup>N. Nagaosa and Y. Tokura, *Nat. Nanotechnol.* **8**, 899 (2013).
- <sup>3</sup>Y. H. Liu and Y. Q. Li, *Chin. Phys. B* **24**, 017506 (2015).
- <sup>4</sup>A. Fert, N. Reyren, and V. Cros, *Nat. Rev. Mater.* **2**, 17031 (2017).
- <sup>5</sup>K. Everschor-Sitte, J. Masell, R. M. Reeve, and M. Kläui, *J. Appl. Phys.* **124**, 240901 (2018).
- <sup>6</sup>S. Mühlbauer, B. Binz, F. Jonietz, C. Pfleiderer, A. Rosch, A. Neubauer, R. Georgii, P. Böni, *Science* **323**, 915 (2009).
- <sup>7</sup>X. Z. Yu, Y. Onose, N. Kanazawa, J. H. Park, J. H. Han, Y. Matsui, N. Nagaosa, and Y. Tokura, *Nature* **465**, 901 (2010).
- <sup>8</sup>S. Seki, X. Z. Yu, S. Ishiwata, and Y. Tokura, *Science* **336**, 198 (2012).
- <sup>9</sup>I. Kézsmárki, S. Bordács, P. Milde, E. Neuber, L. M. Eng, J. S. White, H. M. Rønnow, C. D. Dewhurst, M. Mochizuki, K. Yanai, H. Nakamura, D. Ehlers, V. Tsurkan, and A. Loidl, *Nat. Mater.* **14**, 1116 (2015).
- <sup>10</sup>S. Heinze, K. von Bergmann, M. Menzel, J. Brede, A. Kubetzka, R. Wiesendanger, G. Bihlmayer, and S. Blügel, *Nat. Phys.* **7**, 713 (2011).
- <sup>11</sup>A. K. Nayak, V. Kumar, T. Ma, P. Werner, E. Pippel, R. Sahoo, F. Damay, U. K. Röbner, C. Felser, and S. S. P. Parkin, *Nature (London)* **548**, 561 (2017).
- <sup>12</sup>I. E. Dzyaloshinskii, *J. Phys. Chem. Solids* **4**, 241 (1958); T. Moriya, *Phys. Rev.* **120**, 91 (1960).
- <sup>13</sup>F. Jonietz, S. Mühlbauer, C. Pfleiderer, A. Neubauer, W. Münzer, A. Bauer, T. Adams, R. Georgii, P. Böni, R. A. Duine, K. Everschor, M. Garst, and A. Rosch, *Science* **330**, 1648 (2010).
- <sup>14</sup>J. Iwasaki, M. Mochizuki, and N. Nagaosa, *Nat. Commun.* **4**, 1463 (2013).
- <sup>15</sup>Y. Tchoe and J. H. Han, *Phys. Rev. B* **85**, 174416 (2012).
- <sup>16</sup>Y. Q. Li, Y. H. Liu, and Y. Zhou, *Phys. Rev. B* **84**, 205123 (2011).
- <sup>17</sup>Y. H. Liu and Y. Q. Li, *J. Phys.: Condens. Matter* **25**, 076005 (2013).
- <sup>18</sup>Y. Zhou and M. Ezawa, *Nat. Commun.* **5**, 4652 (2014).
- <sup>19</sup>M. Mochizuki, X. Z. Yu, S. Seki, N. Kanazawa, W. Koshibae, J. Zang, M. Mostovoy, Y. Tokura, and N. Nagaosa, *Nat. Mater.* **13**, 241 (2014).
- <sup>20</sup>L. Kong and J. Zang, *Phys. Rev. Lett.* **111**, 067203 (2013).
- <sup>21</sup>S.-Z. Lin, C. D. Batista, C. Reichhardt, and A. Saxena, *Phys. Rev. Lett.* **112**, 187203 (2014).
- <sup>22</sup>W. Wang, M. Beg, B. Zhang, W. Kuch, and H. Fangohr, *Phys. Rev. B* **92**, 020403 (2015).
- <sup>23</sup>M. Ikka, A. Takeuchi, and M. Mochizuki, *Phys. Rev. B* **98**, 184428 (2018).
- <sup>24</sup>Y. Nii, T. Nakajima, A. Kikkawa, Y. Yamasaki, K. Ohishi, J. Suzuki, Y. Taguchi, T. Arima, Y. Tokura, and Y. Iwasa, *Nat. Commun.* **6**, 8539 (2015).
- <sup>25</sup>P.-J. Hsu, A. Kubetzka, A. Finco, N. Romming, K. von Bergmann, and R. Wiesendanger, *Nat. Nanotechnol.* **12**, 123 (2017).
- <sup>26</sup>C. Ma, X. Zhang, J. Xia, M. Ezawa, W. Jiang, T. Ono, S. N. Piramanayagam, A. Morisako, Y. Zhou, and X. Liu, *Nano Lett.* **19**, 353 (2019).
- <sup>27</sup>J. S. White, I. Levatić, A. A. Omrani, N. Egetenmeyer, K. Prša, I. Živković, J. L. Gavilano, J. Kohlbrecher, M. Bartkowiak, H. Berger, and H. M. Rønnow, *J. Phys.: Condens. Matter* **24**, 432201 (2012).
- <sup>28</sup>M. Mochizuki and Y. Watanabe, *Appl. Phys. Lett.* **107**, 082409 (2015).
- <sup>29</sup>K. Nawaoka, S. Miwa, Y. Shiota, N. Mizuochi, and Y. Suzuki, *Appl. Phys. Express* **8**, 063004 (2015).
- <sup>30</sup>T. Srivastava, M. Schott, R. Juge, V. Křížáková, M. Belmeguain, Y. Roussigné, A. Bernard-Mantel, L. Ranno, S. Pizzini, S. Chérif, A. Stashkevich, S. Auffret, O. Boulle, G. Gaudin, M. Chshiev, C. Baraduc, and H. Béa, *Nano Lett.* **18**, 4871 (2018).
- <sup>31</sup>M. Garst, J. Waizner, and D. Grundler, *J. Phys. D: Appl. Phys.* **50**, 293002 (2017).
- <sup>32</sup>M. Mochizuki and S. Seki, *J. Phys.: Condens. Matter* **27**, 503001 (2015).
- <sup>33</sup>M. Mochizuki, *Phys. Rev. Lett.* **108**, 017601 (2012).
- <sup>34</sup>Y. Onose, Y. Okamura, S. Seki, S. Ishiwata, and Y. Tokura, *Phys. Rev. Lett.* **109**, 037603 (2012).
- <sup>35</sup>Y. Okamura, F. Kagawa, M. Mochizuki, M. Kubota, S. Seki, S. Ishiwata, M. Kawasaki, Y. Onose, and Y. Tokura, *Nat. Commun.* **4**, 2391 (2013).
- <sup>36</sup>T. Schwarze, J. Waizner, M. Garst, A. Bauer, I. Stasinopoulos, H. Berger, C. Pfleiderer, D. Grundler, *Nat. Mater.* **14**, 478 (2015).
- <sup>37</sup>D. Ehlers, I. Stasinopoulos, V. Tsurkan, H.-A. Krug von Nidda, T. Fehér, A. Leonov, I. Kézsmárki, D. Grundler, and A. Loidl, *Phys. Rev. B* **94**, 014406 (2016).
- <sup>38</sup>P. Padmanabhan, F. Sekiguchi, R. B. Versteeg, E. Slivina, V. Tsurkan, S. Bordács, I. Kézsmárki, and P. H. M. van Loosdrecht, *Phys. Rev. Lett.* **122**, 107203 (2019).
- <sup>39</sup>M. Mochizuki and S. Seki, *Phys. Rev. B* **87**, 134403 (2013).
- <sup>40</sup>Y. H. Liu, Y. Q. Li, and J. H. Han, *Phys. Rev. B* **87**, 100402(R)

- (2013).
- <sup>41</sup>K. Siratori and E. Kita, *J. Phys. Soc. Jpn.* **48**, 1443 (1980).
- <sup>42</sup>T. Liu and G. Vignale, *Phys. Rev. Lett.* **106**, 247203 (2011).
- <sup>43</sup>W. Chen and M. Sigrist, *Phys. Rev. Lett.* **114**, 157203 (2015).
- <sup>44</sup>D. L. Mills and I. E. Dzyaloshinskii, *Phys. Rev. B* **78**, 184422 (2008).
- <sup>45</sup>A. Takeuchi and M. Mochizuki, *Appl. Phys. Lett.* **113**, 072404 (2018).
- <sup>46</sup>B. Berg and M. Lüscher, *Nucl. Phys. B* **190**, 412 (1981).
- <sup>47</sup>V. Flovik, A. Qaiumzadeh, A. K. Nandy, C. Heo, and Theo Rasing, *Phys. Rev. B* **96**, 140411(R) (2017).
- <sup>48</sup>V. L. Zhang, C. G. Hou, K. Di, H. S. Lim, S. C. Ng, S. D. Pollard, H. Yang, and M. H. Kuok, *AIP Adv.* **7**, 055212 (2017).